Binder Jetting Additive Manufacturing: Effect of Particle Size Distribution on Density

Wenchao Du [a], Jorge Roa [b], Jaehee Hong [b], Yanwen Liu [c], Zhijian Pei [a], and *Chao Ma [a,b,c]

[a] Department of Industrial & Systems Engineering, Texas A&M University, College Station, TX

[b] Department of Engineering Technology & Industrial Distribution, Texas A&M University, College Station, TX

[c] Department of Mechanical Engineering, Texas A&M University, College Station, TX

Abstract

This paper reports a study on the effects of particle size distribution (tuned by mixing different-sized powders) on density of a densely packed powder, powder bed density, and sintered density in binder jetting additive manufacturing. An analytical model was used first to study the mixture packing density. Analytical results showed that multimodal (bimodal or trimodal) mixtures could achieve a higher packing density than their component powders and there existed an optimal mixing fraction to achieve the maximum mixture packing density. Both a lower component particle size ratio (fine to coarse) and a larger component packing density ratio (fine to coarse) led to a larger maximum mixture packing density. A threshold existed for the component packing density ratio, below which the mixing method was not effective for density improvement. Its relationship to the component particle size ratio was calculated and plotted. In addition, the dependence of the optimal mixing fraction and maximum mixture packing density on the component particle size ratio and component packing density ratio was calculated and plotted.

*Corresponding author: cma@tamu.edu

Some of the experimental data used in this paper were also used in a conference paper that was published in the Proceedings of the ASME 2018 13th International Manufacturing Science and Engineering Conference, MSEC2018-6651.

These plots can be used as theoretical tools to select parameters for the mixing method. Experimental results of tap density were consistent with the above-mentioned analytical predictions. Also, experimental measurements showed that powders with multimodal particle size distributions achieved a higher tap density, powder bed density, and sintered density in most cases.

1 Introduction

Additive manufacturing (AM), also known as 3D printing, can be described as a process of joining materials with a primary objective of making objects from 3D model data using a layer-by-layer principle [1,2]. Binder jetting is one of the most advantageous technologies to produce large complex-shaped parts due to its capability of processing various materials [3–5], no need for explicit support structure [6], and high scalability [7,8]. Since the first paper on binder jetting [9], a number of studies have been reported on processing of different materials such as ceramics [3] and metals [4], and fabrication of different products such as load-bearing parts [10–13] and biomedical parts [14–16].

The particle size distribution of feedstock powder affects the powder packing density and the sintered density [17]. Particle size distribution can be tuned by mixing different-sized powders. For example, Sun et al. studied the effects of particle size distribution on the bulk density of sintered samples [18]. Glass-ceramic powders with two size ranges (45–100 μm and 0–25 μm) were mixed in fractions of 90:10, 80:20, 70:30, and 60:40, respectively. The mixture with the fraction of 60:40 achieved the highest sintered density of 1.60 g/cm^3. Bai et al. also investigated the effect of particle size distribution [19]. A bimodal mixture from powders with particle sizes of 30 and 5 μm and a mixing ratio of 73:27 achieved an improved tap density (by 8.3%) and sintered density (by ~8%) compared with the component powders. However, no research has been done to

investigate the theoretically achievable packing density by mixing different-sized powders and compare it with experimentally obtained results. This work aims to fill this knowledge gap.

Particle packing is of interest in many fields, such as civil engineering [20]. For a mixture of different-sized component powders, analytical models have been developed to predict the mixture packing density using the size, volume fraction, and packing density of each component powder. Compared with numerical methods such as the discrete element method, an analytical method has its own advantages such as low computational cost and explicit solutions [21]. The linear packing model, proposed by Stovall et al. [22], is one of the most popular analytical models [23,24].

The objective of this research is to examine the effects of particle size distribution on density of a densely packed powder, powder bed density, and sintered density with both analytical and experimental methods. Firstly, the analytical linear packing model was employed to study the effects of various parameters (mixing fraction, component particle size ratio, and component packing density ratio) on the mixture packing density. Afterward, the analytical model was used to predict the mixture packing density from selected component powders (70, 10, and 2 μm powders) under the ideal conditions (i.e., the state of dense packing). Afterward, experimental studies were conducted to evaluate the actual conditions. Tap density, powder bed density, and sintered density of each component and mixture were measured and compared with the analytical results. Although ceramic is selected as the model material and binder jetting is selected as the model AM technology, this mixing method maintains its potentiality for other materials (such as metals and composites) and other AM technologies (such as powder bed fusion).

2 Analytical Method

The analytical linear packing model assumes that all component powders and mixtures are composed of non-deformable particles under the state of dense packing [22]. In the case of a mixture with n component powders (the component powders are ranked such that $d_i \geq d_{i+1}$, where d_i is the diameter of the ith component), the mixture packing density is given by [16]

$$\gamma = \min(\gamma_1, \gamma_2, \cdots, \gamma_n) \tag{1}$$

where γ_i is a specific mixture packing density when the ith component is "dominant" [22] and given by

$$\gamma_i = \frac{\beta_i}{1 - \sum_{j=1}^{i-1}\left[1 - \beta_i + b_{i,j}\beta_i\left(1 - \frac{1}{\beta_j}\right)\right]y_j - \sum_{j=i+1}^{n}\left[1 - a_{i,j}\frac{\beta_i}{\beta_j}\right]y_j} \tag{2}$$

where β_i and y_i are the packing density and volume fraction of the ith component, respectively, and $a_{i,j}$ and $b_{i,j}$ are interaction functions which are called loosening and wall effect parameters, respectively. In the linear packing model, the loosening effect is referred to as a phenomenon that fine particles loosen the packing of coarse particles when squeezing themselves into the space that is near the contact point between two coarse particles and making coarse particles more dispersed. The wall effect describes how coarse particles disrupt the packing of fine particles at wall-like boundaries of coarse particles [23]. Both these effects decrease the packing density. Interaction functions derived from a curve fitting of experimental results by de Larrard [24] are

$$a_{i,j} = \sqrt{1 - \left(1 - \frac{d_j}{d_i}\right)^{1.02}} \tag{3}$$

$$b_{i,j} = 1 - \left(1 - \frac{d_j}{d_i}\right)^{1.5} \quad (4)$$

2.1 Parametric study on binary mixing

2.1.1 Effect of mixing fraction on mixture packing density

Mixing fraction is an important parameter that affects the mixture packing density. In a binary mixing, the mixing fraction can be described with the volume fraction of either the coarse or fine powder, y_1 or y_2 in Equation (2). In the parametric study on binary mixing, the coarse powder fraction was used, which was varied from 0 vol.% to 100 vol.% (corresponding to 100 vol.% to 0 vol.% for the fine powder fraction) with an increment of 0.01 vol.%. The component particle size ratio, d_2/d_1 in Equations (3) and (4), was set as 0.1. The packing density of both the coarse and fine raw powders, β_1 and β_2 in Equation (2), was set to 63.7%. This packing density value is common for a densely packed powder [25,26].

2.1.2 Effect of component particle size ratio on mixture packing density

The effect of component particle size ratio (fine to coarse), d_2/d_1 in Equations (3) and (4), was studied by varying it from 1/2, 1/4, 1/8, 1/16, to 1/32. This parametric study was performed over the full range of the coarse powder fraction, i.e., 0 vol.% to 100 vol.% with an increment of 0.01 vol.%. The packing density of both coarse and fine raw powders, β_1 and β_2 in Equation (2), was set to 63.7%.

2.1.3 Effect of component packing density ratio on mixture packing density

Component packing density of coarse and fine raw powders, β_1 and β_2 in Equation (2), respectively, is another important parameter that affects the mixture packing density. To simplify

the analysis, a component packing density ratio (fine to coarse) was defined, β_2/β_1. The coarse powder packing density (β_1) was set to 63.7%. The component packing density ratio was varied from 0.5 to 1.0 by changing the fine powder packing density (β_2) accordingly. This parametric study was performed over the full range of the coarse powder fraction, i.e., 0 vol.% to 100 vol.% with an increment of 0.01 vol.%. The component particle size ratio (d_2/d_1) was set to 1/3.

2.1.4 Relationship between critical component packing density ratio and component particle size ratio

Component particle size ratio could have double-edged effects on the mixture packing density. A smaller component particle size ratio could strengthen the filling effect of the fine powder and thus lead to a higher mixture packing density. However, a smaller component particle size ratio is usually associated with a lower packing density of the fine powder given the same coarse powder, which could lead to a lower mixture packing density. Therefore, the effectiveness of the mixing method, i.e., whether it improves the packing density, depends on the component packing density ratio given a component particle size. Given a component particle size ratio, if the component packing density ratio is below a certain threshold, defined as the critical component packing density ratio, the mixing method does not improve the packing density, regardless of the mixing fraction. The objective of this parametric study is to determine the relationship between the critical component packing density ratio and the component particle size ratio. In this study, the packing density of the coarse powder (β_1) was set to 63.7%.

2.1.5 Optimal mixing fraction and maximum mixture packing density

Lastly, the model was used to predict the optimal mixing fraction and the maximum mixture packing density. In this study, the component particle size ratio was varied from 0.001 to 0.5 with

an increment of 0.0005. The component packing density ratio was varied from 0.5 to 1.0 with an increment of 0.1.

2.2 Case study on ternary mixing

Due to the large number of parameters involved in ternary mixing than in binary mixing, ternary mixing was analytically investigated as a case study for the powders used in the experiments. Tap density of the selected component powders were measured (described in Section 3.3) and used as the inputs of the analytical model. A ternary plot was used to illustrate the packing density values at all compositions.

3 Experimental Methods

3.1 Powder preparation

Three spherical alumina powders (Inframat, CT, USA) of different particle sizes (2, 10, and 70 μm, respectively) were selected as component powders. To prepare multimodal mixtures, the component powders were weighted using a balance with an accuracy of 0.1 mg (AGCN200, Torbal, USA) and mixed using ball milling (Jar Rolling Mills, Paul O. Abbe, USA) with parameters listed in Table 1. Alumina balls, same as the powder material, were employed to avoid contamination. Small balls and low milling speed were used to avoid breaking the particles.

Table 1. Parameters used in ball milling

Parameter	Value
Ball-to-powder weight ratio	1:10
Ball diameter (mm)	2
Normalized mill rotation speed (%)	30
Milling time (h)	1

3.2 Characterization of powder morphology

The morphology of all component powders and mixtures was characterized using scanning electron microscopy (SEM, TESCAN VEGA II LSU, Brno-Kohoutovice, Czech).

3.3 Measurement of tap density

Tap density is considered as a good estimation for the density of a densely packed powder [27,28]. Tap density was measured by following an ASTM standard [29]. A tap density meter (DY-100A, Hongtuo, China) was used. In each measurement, 100 g of powder was tapped with a 3-mm stroke for 3000 cycles. After tapping, the powder mass was divided by the powder volume to obtain the absolute tap density, which was then divided by the theoretical density of alumina (3.97 g/cm^3 [30]) to obtain the relative tap density.

3.4 Measurement of powder bed density

Powder bed density was determined by spreading ten layers of powder using a lab-designed setup (as shown in Figure 1) and measuring the mass and volume of the spread layers. This method has been widely used in other studies [31,32]. The layer thickness was 130 μm. The forward rotating roller had a diameter of 5 cm and a smooth glass surface. The process started with powder spreading with the roller. After one powder layer was spread, the lead screw was rotated to lower the build platform for another powder layer. No binder was applied in this measurement to avoid its interference with the measurement of powder bed density. The total height of the powder bed was measured by a caliper (with an accuracy of 10 μm). Afterward, all powder inside the chamber of the setup was carefully collected, and the mass of the collected powder was measured by a balance with an accuracy of 0.1 mg (AGCN200, Torbal, USA). The volume of the powder layers was calculated based on the inner diameter of the chamber and the total height of the powder bed.

The total mass of the collected powder was divided by the total volume to obtain the powder bed density. This process was repeated three times for each powder.

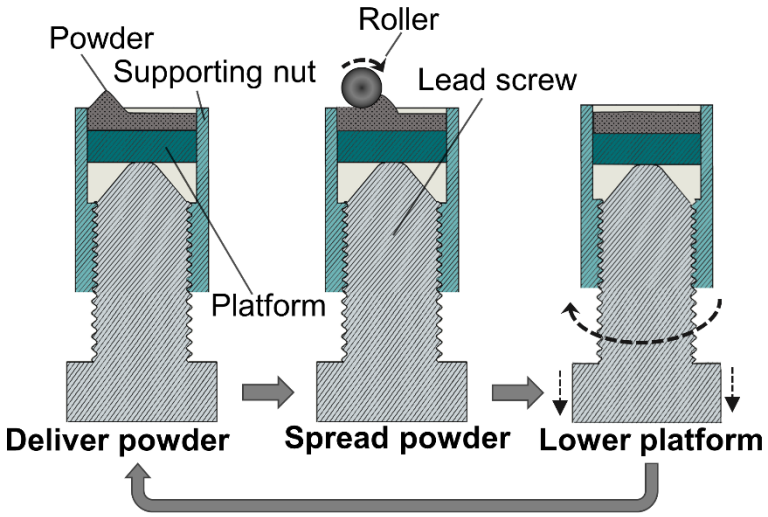

Figure 1. Powder spreading process with a lab-designed setup

3.5 Printing and sintering

Printing experiments were carried out using the lab-designed setup, as illustrated in Figure 2. The process started with powder spreading using the forward rotating roller with a diameter of 5 cm to form the first foundation layer. Then the lead screw was rotated to lower the build platform. The layer thickness was 130 μm. Totally, two foundation layers were spread without jetting any binder. Afterward, the first powder layer for printing was spread, and then the powder bed was covered by a mask with an opening corresponding to the cross section of the desired shape, which was a circle with a diameter of 10 mm in this case. The printing binder was an aqueous solution containing 3 wt.% polyvinyl alcohol (molecule weight of 31,000), and 0.33 g of binder was applied for each powder layer. Then the mask was removed and the platform was lowered by a distance equal to the layer thickness (130 μm). This process was repeated until an entire disk-shaped green sample was printed. The print was repeated three times for each powder.

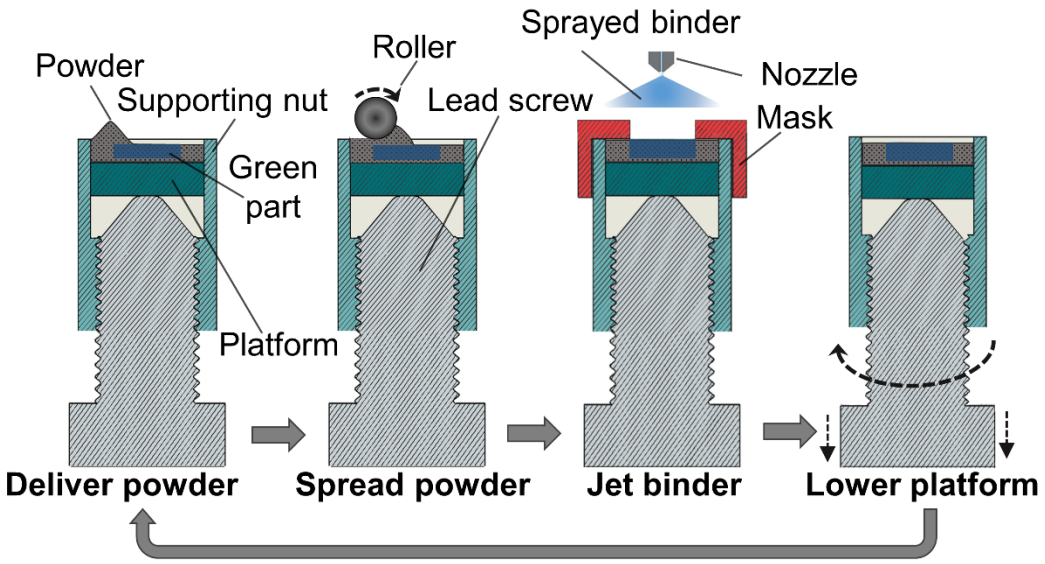

Figure 2. Binder jetting additive manufacturing process with a lab-designed setup

After printing, the samples were cured in a low-temperature furnace (KSL-1100X-S-UL-LD, MTI Corporation, USA) at 200 °C for 2 h to evaporate the water in the binder and join the particles. After cooling, the green samples were carefully extracted from the powder bed and placed in a high-temperature furnace (KSL-1700X-A2-UL, MTI Corporation, USA) for debinding and sintering. The furnace temperature was increased to 350 °C at a ramp-up rate of 5 °C/min, followed by debinding from 350 °C to 550 °C at a ramp-up rate of 1 °C/min. Then the samples were heated up to 1600 °C at 5 °C/min and sintered for 2 h, followed by cooling to the room temperature. All these post-processing procedures were performed in air.

3.6 Measurement of sintered density

Density of sintered samples was measured with the Archimedes' method. After a dry mass (m_d) measurement, each sample was carefully lowered onto a pan suspended in a beaker of deionized water to determine its wet mass (m_w). The mass measurements were done using a balance

with an accuracy of 0.1 mg (AGCN200, Torbal, USA). The dry and wet masses were then used to calculate the density of the samples using the following equation:

$$\rho_{sp} = \rho_{wt} \frac{m_d}{m_d - m_w} \quad (5)$$

where ρ_{sp} is the sintered density and ρ_{wt} is the water density at the experimental temperature. If a sample has a high porosity, the water infiltrates the sample and thus the above method overestimates the density. Therefore, all samples were coated with an extremely thin layer of wax to prevent the water from infiltrating the samples.

3.7 Characterization of sintered microstructure

The microstructure of sintered samples was characterized using SEM (TESCAN VEGA II LSU, Brno-Kohoutovice, Czech).

4 Analytical Results and Discussion

4.1 Parametric study on binary mixing

4.1.1 Effect of mixing fraction on mixture packing density

The modeling results of the effect of mixing fraction are shown in Figure 3. The mixture packing density increases first and then decreases as the coarse powder fraction increases. A maximum value of the mixture packing density (i.e., maximum mixture packing density) exists for a certain coarse powder fraction (i.e., the optimal fraction of coarse powder). This trend can be explained from the perspective of either the fine powder or the coarse powder. On one hand, the increase of the fine powder fraction (from right to left for the X-axis in Figure 3) lets more fine particles fill into the voids among the coarse particles and consequently increases the packing density, which is the so-called filling effect of the fine powder [22,33]. However, after all voids

are filled, the introduction of more fine particles decreases the packing density due to the loosening effect of the fine powder [22,33]. On the other hand, the increase of the coarse powder fraction (from left to right for the X-axis in Figure 3) allows a single coarse particle to replace multiple fine particles and completely fill the voids among them, consequently increasing the packing density, which is the so-called occupying effect of the coarse powder [22,33]. However, after available voids are occupied by coarse particles, the packing density decreases due to the wall effect of the coarse powder [22,33].

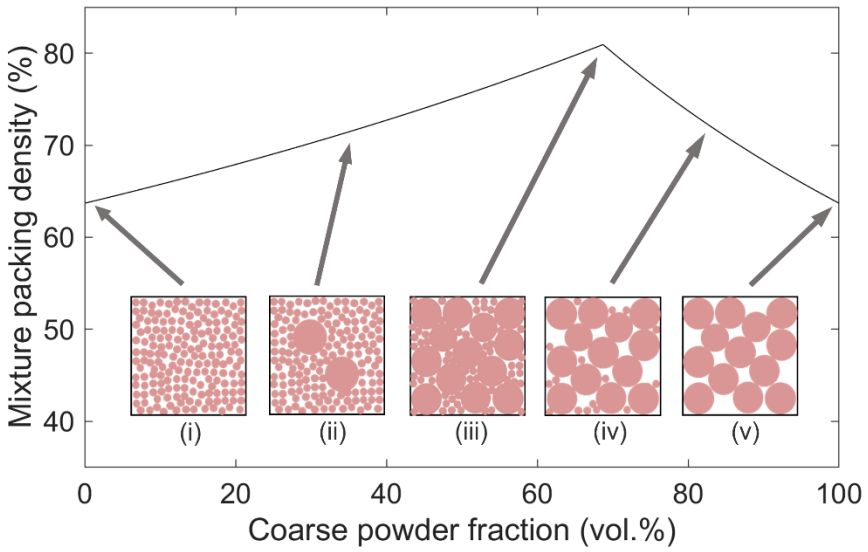

Figure 3. Bimodal mixture packing density dependent on coarse powder fraction when the component particle size ratio is 0.1 and the packing density of the fine and coarse powders is 63.7%

4.1.2 Effect of component particle size ratio on mixture packing density

The modeling results of the effect of component particle size ratio are shown in Figure 4. For the same coarse powder fraction in Figure 4, a smaller particle size ratio leads to a larger mixture packing density. As the particle size ratio decreases (i.e., the fine particles become smaller

considering the same coarse powder), the fine particles have less geometric constrain and thus can fill more space among the coarse particles (e.g., near the contact point between two coarse particles).

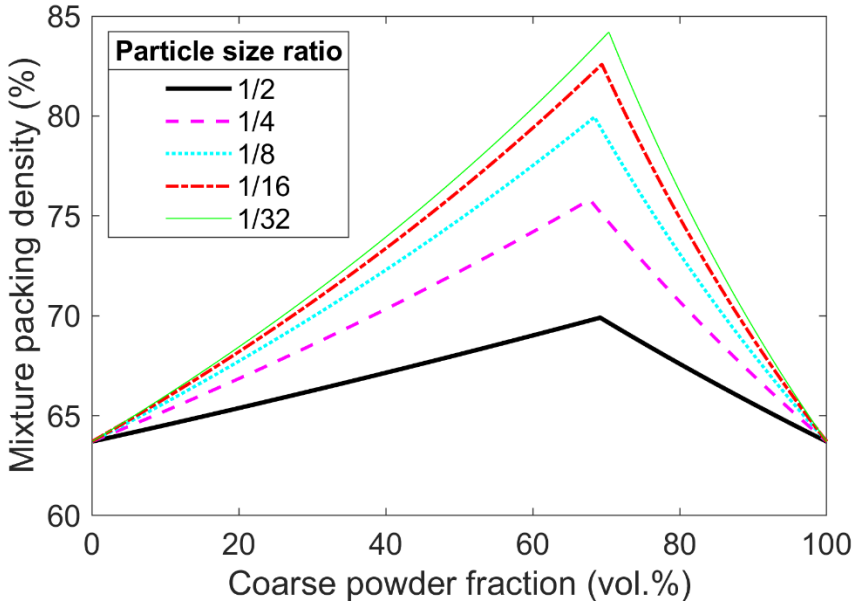

Figure 4. Bimodal mixture packing density dependent on component particle size ratio when the packing density of the fine and coarse powders is 63.7%

4.1.3 Effect of component packing density ratio on mixture packing density

The modeling results of the effect of component packing density ratio are illustrated in Figure 5. Since the fine powder packing density is varied while the coarse powder packing is kept at the same, all curves have different starting points but the same ending point. When the packing density ratio decreases, the mixture packing density decreases. This is because fewer fine particles can be inserted into the voids among the coarse particles.

Interestingly, when the packing density ratio is low (i.e., 0.5), the mixture packing density increases monotonically as the coarse powder fraction increases (i.e., as the fine powder fraction

decreases). It means that when the fine powder packing density is too low, adding any amount of fine powder into the coarse powder will loosen its packing.

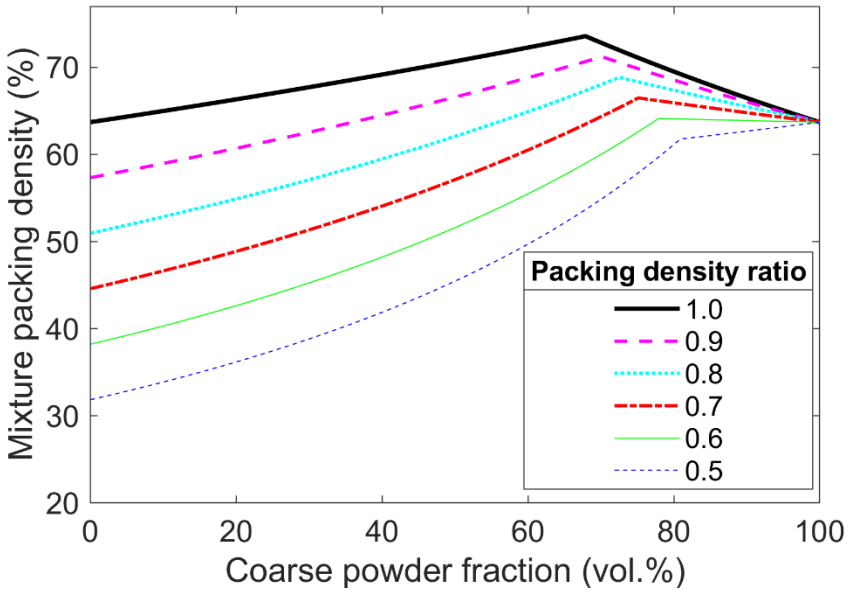

Figure 5. Bimodal mixture packing density dependent on component packing density ratio when the component particle size ratio is 1/3

4.1.4 Relationship between critical component packing density ratio and component particle size ratio

The relationship between the critical component packing density ratio and the component particle size ratio is shown in Figure 6. Before mixing, this figure can be used to determine if the mixing method improves the packing density in comparison with the coarse powder, given a combination of particle size ratio and packing density ratio. After measuring the packing densities and particle sizes of two component powders, a point in Figure 6 can be located. Depending on whether the point is located to the left or right of the curve, it can be determined whether the mixing method improves the packing density or not.

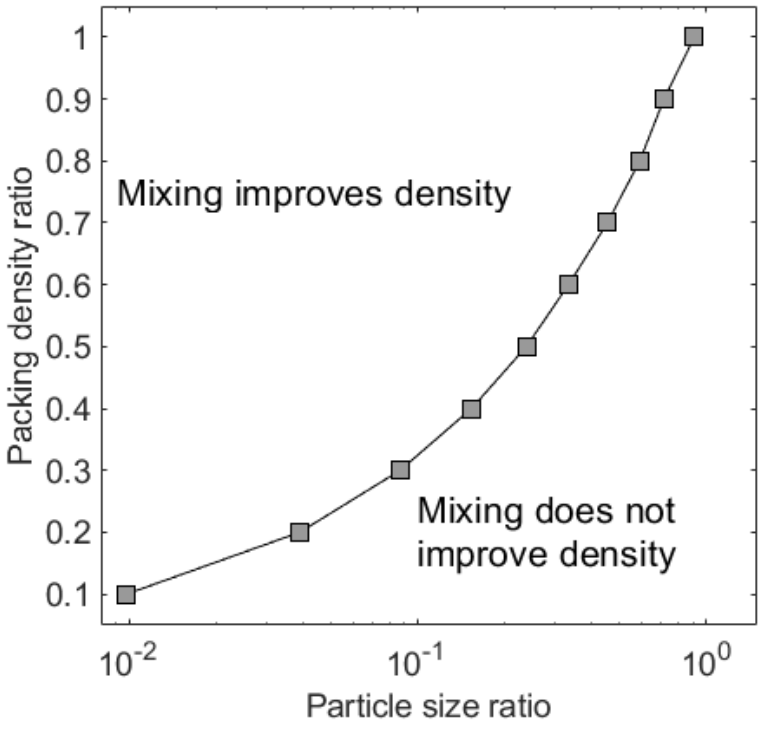

Figure 6. Relationship between critical component packing density ratio and component particle size ratio

4.1.5 Optimal mixing fraction and maximum mixture packing density

The dependence of the optimal fraction of coarse powder on the component particle size ratio and packing density ratio is shown in Figure 7(a). The optimal fraction of coarse powder decreases as the packing density ratio increases. This is due to the higher packing density of the fine powder and consequently more fine particles that can be packed into the voids among coarse particles, leading to the decrease of the optimal fraction of coarse powder.

In Figure 7(a), although all curves follow a similar overall trend, the optimal fraction of coarse powder behaves slightly differently between the small (0.5–0.7) and large (0.8–1.0) component packing density ratios at a high (0.25–0.5) component particle size ratio. At a small packing density ratio and a high particle size ratio, the optimal fraction is 100 vol.%. This means the coarse powder

has a higher packing density than any bimodal mixture. It further indicates that the mixing method does not improve the packing density if the fine powder has a similar particle size but a lower packing density than the coarse powder, which agrees with the results in Figure 6.

The effects of the component particle size ratio and component packing density ratio on the maximum mixture packing density are illustrated in Figure 7(b). The maximum mixture packing density is a monotonically decreasing function of the particle size ratio. This is due to the more geometric constrain of the fine particles. For the same particle size ratio, the maximum mixture packing density increases as the packing density ratio increases. This is due to the higher packing density of the fine powder. Similar to Figure 7(a), the maximum mixture packing density is 63.7% when the particle size ratio is large (0.25–0.5) and the packing density ratio is small (0.5–0.7), indicating that mixing method does not improve the packing density under these conditions.

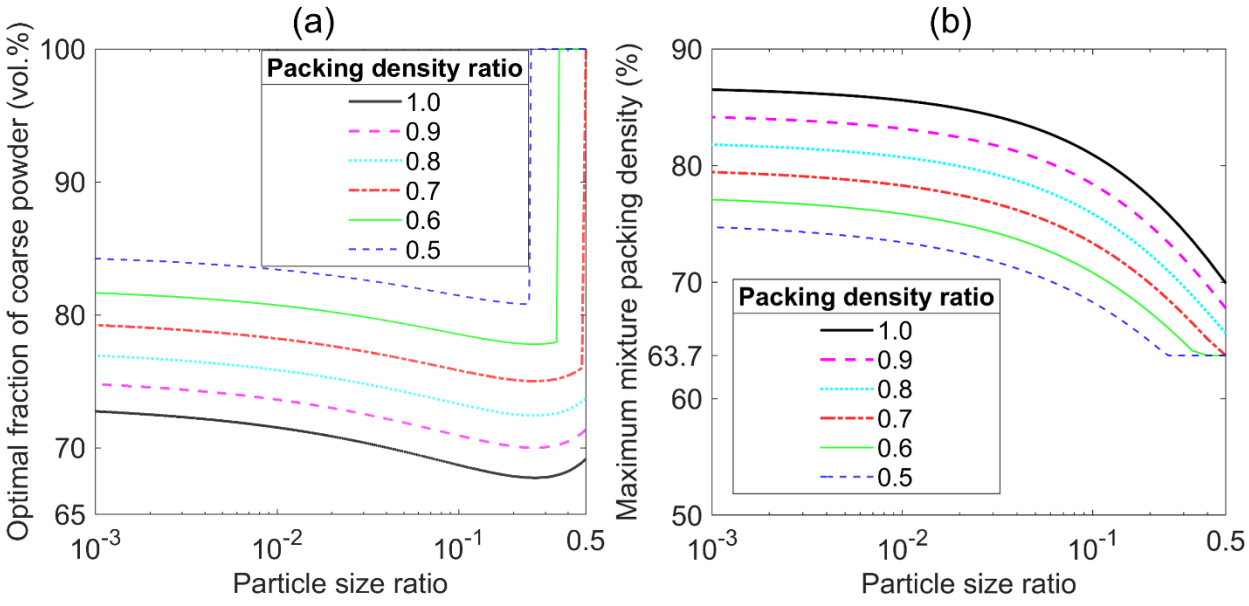

Figure 7. (a) Optimal fraction of coarse powder and (b) maximum mixture packing density of bimodal mixture dependent on component particle size ratio and packing density ratio

4.2 Case study on ternary mixing

Tap density of three component powders is listed in Table 2. The fine powders (10 μm and 2 μm) have a slightly lower tap density than the coarse powder (70 μm) because they have higher inter-particle cohesion [27], which makes them slightly more difficult to be densely compacted.

Table 2. Tap density of component powders

Powder particle size (μm)	Absolute tap density (g/cm^3)	Relative tap density (%)
70	2.47	62.2
10	2.42	61.0
2	2.42	61.0

Figure 8 shows a ternary plot containing the modeled packing density of bimodal (i.e., 10/2, 70/10, 70/2) and trimodal (i.e., 70/10/2) mixtures. Each point in the ternary plot represents a composition of the three component powders. The left, right and bottom sides are volume fractions of the component powders of 70 μm, 10 μm, and 2 μm, respectively. The left, right and top vertexes represent the full fraction (100 vol.%) for the component powders of 2 μm, 10 μm, and 70 μm, respectively. Fractions for a specific mixture can be determined by drawing a line through the mixture point parallel to the opposite side of component vertex and intersecting the component axis. The trimodal mixture that achieves the highest packing density is marked as a red dot in the plot as an example. The fraction of the 70-μm powder is determined by drawing a parallel line to the bottom side. The intersection of the left side and the parallel line is the fraction, which is 61.3 vol.%. Similarly, the fractions of 10-μm and 2-μm component powders are determined, which are 21.1 vol.% and 17.6 vol.%, respectively. Moreover, three sides of the triangle represent three bimodal mixtures (i.e., trimodal mixtures with a zero fraction of the corresponding vertex component), and their modeled results are plotted along the sides. The bimodal mixtures that

achieve the highest packing densities are also marked as red dots. The optimal mixing fraction and the maximum packing density for the bimodal and trimodal mixtures are listed in Table 3.

The packing density of a trimodal mixture has a similar dependence on the mixing faction to that of a bimodal mixture (increases first and then decreases) if one component fraction is kept constant and the other two component fractions are varied, as shown by the grey dashed lines inside the ternary plot in Figure 8. Furthermore, a trimodal mixture does not always have a higher packing density than a bimodal mixture. For example, the trimodal mixtures near the three corners of the ternary plot have a lower packing density than the three red dots on the edges. However, it can be concluded that the multimodal mixture always has a higher packing density than at least one of its component powders. In a proper mixing fraction range, the packing density of the multimodal mixture is higher than that of any of its component powders.

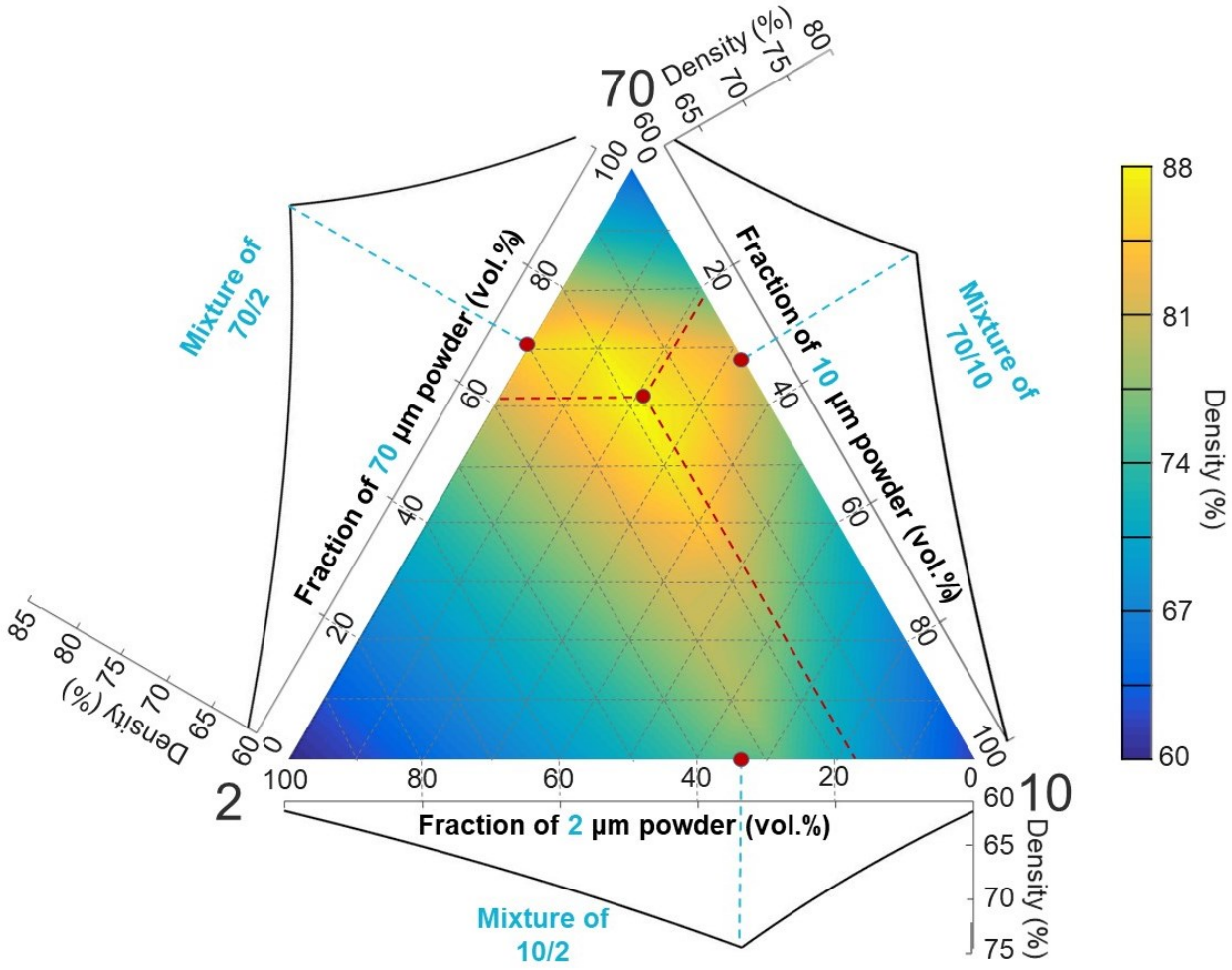

Figure 8. Modeled trimodal mixture packing density dependent on fractions of three component powders (70, 10, and 2 µm)

Table 3. Analytical results from case study

Bimodal or trimodal mixture	Optimal mixing fraction (vol.%)	Maximum mixture packing density (%)
10/2	66.3:33.7	74.8
70/10	67.7:32.3	77.4
70/2	70.0:30.0	82.6
70/10/2	61.3:21.1:17.6	85.7

5 Experimental Results and Discussion

5.1 Powder morphology

Figure 9 shows the particle morphology of three component powders. The shapes are primarily spherical, and the sizes are not perfectly uniform. In this paper, the average sizes were used since the size variation within each component powder was much smaller than the differences across these three component powders.

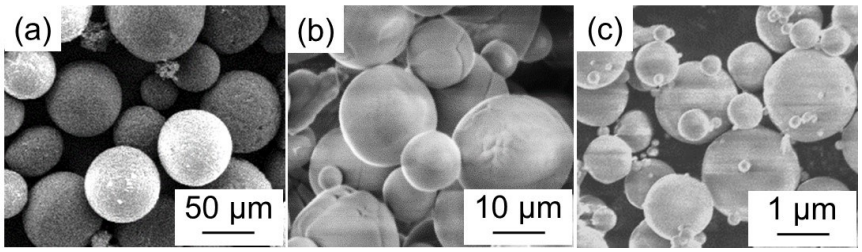

Figure 9. Micrographs of component powders: (a) 70 µm, (b) 10 µm, and (c) 2 µm

Figure 10 shows the SEM images of four multimodal mixtures whose compositions are listed in Table 3. The fine particles can be found in the voids among the coarse particles.

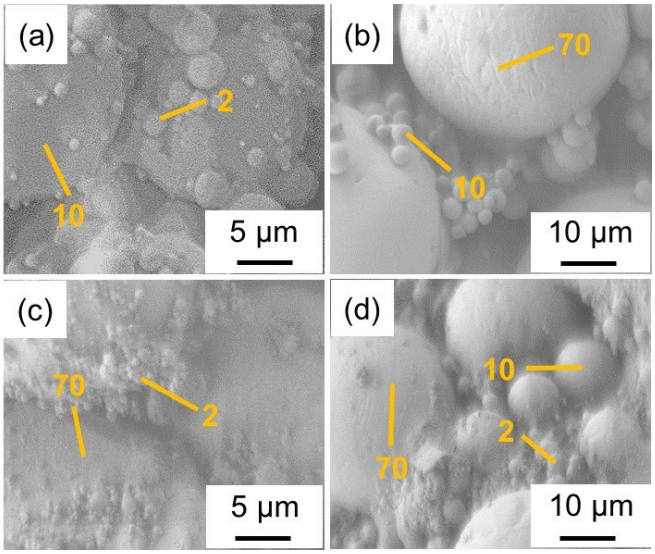

Figure 10. Micrographs of multimodal mixtures: (a) 10/2, (b) 70/10, (c) 70/2, and (d) 70/10/2

5.2 Tap density

The tap density results of three bimodal mixtures with different mixing fractions are shown in Figure 11. The trend from the experimental results agrees well with that from the analytical prediction in Figure 3. As the coarse powder fraction increases, the tap density increased first and then decreased. It can also be concluded that a smaller component particle size ratio leads to a larger mixture tap density, which agrees with the analytical prediction in Figure 4.

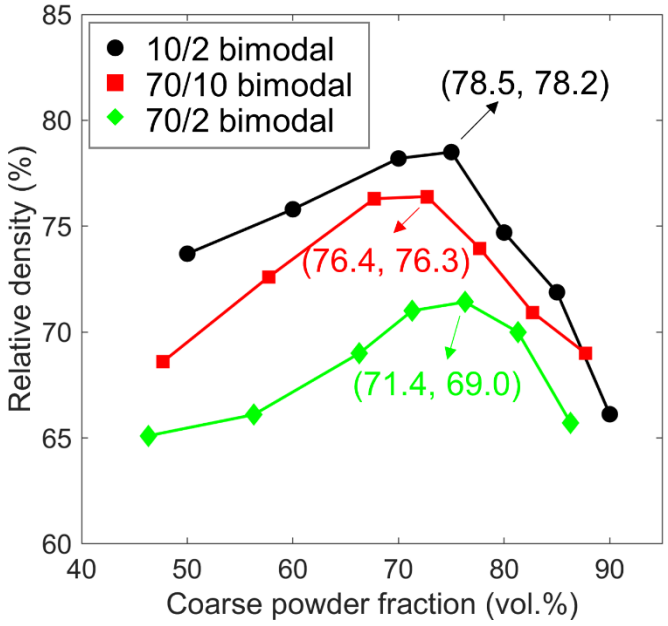

Figure 11. Experimental results of tap density for bimodal mixtures

Figure 12 shows the interpolation of the tap density for the trimodal (and bimodal) powders (marked as grey dots). Approaches to determining the trimodal mixing fractions for a specific point on the plot are descripted in Section 4.2. The overall trend from the experimental results agrees well with that from the analytical prediction in Figure 8. When one component fraction is unchanged and the other two are varied, the tap density of the trimodal mixture shows a similar trend as that of bimodal mixture. For example, when the fraction of 10 μm powder is maintained at 20 vol.% and the fraction of 70 μm powder increased from 40 vol.% to 50 vol.% and then to 60 vol.%, the tap density increased from 75.3% to 79.0% and then decreased to 78.2%. The maximum tap density from all tested trimodal mixtures is 81.6%, which is larger than that of all bimodal mixtures.

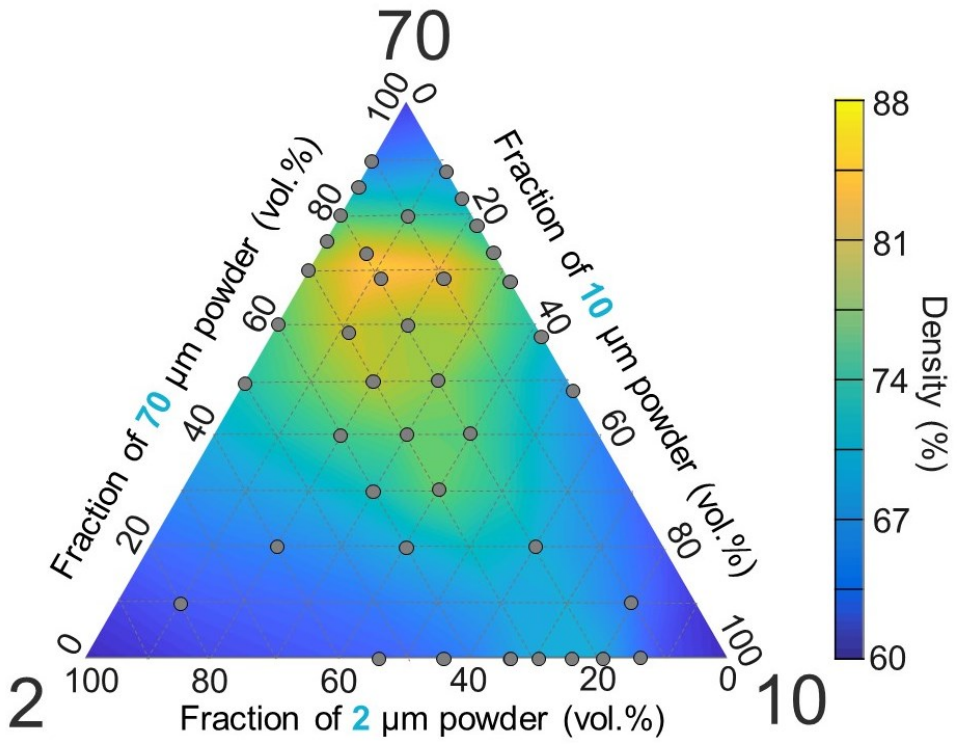

Figure 12. Tap density of trimodal (and bimodal) mixtures at different fractions of three component powders

Figure 13 shows the deviation of the bimodal mixture packing density predicted by the analytical model from the experimentally measured tap density. For each bimodal mixture, the deviation has relatively large positive values at a low coarse powder fraction, indicating an overestimation by the analytical model. A possible reason is the effect of the fine powder, which is more loosely packed after tapping. As the coarse powder fraction increases, the effect of the fine powder becomes less significant, leading to smaller deviation values.

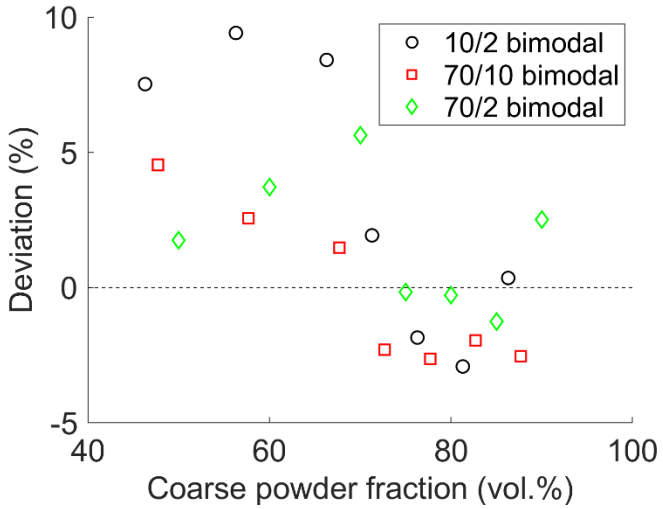

Figure 13. Deviation of bimodal mixture packing density predicted by the analytical model from measured tap density

Similarly, Figure 14 shows the deviation of predicted mixture packing density from the experimentally measured tap density for the trimodal mixture. Approaches to determining the trimodal mixing fractions for a specific point on the plot are descripted in Section 4.2. The ternary plot shows a large portion area of yellow and red colors, indicating that the analytical results are larger than those of the experimental ones. The area close to the bottom line (i.e., mixtures with a relatively small fraction of 70-μm powder and a relatively large fraction of 2-μm powder) shows higher deviation values than other areas.

The mismatch associated with the fine powders (powders with particle sizes of 10 and 2 μm) may be because the analytical model does not consider inter-particle cohesion and satellite particles. In this case, the discrete element method will be advantageous due to its microscopic nature [21]. This method will be considered in the future work.

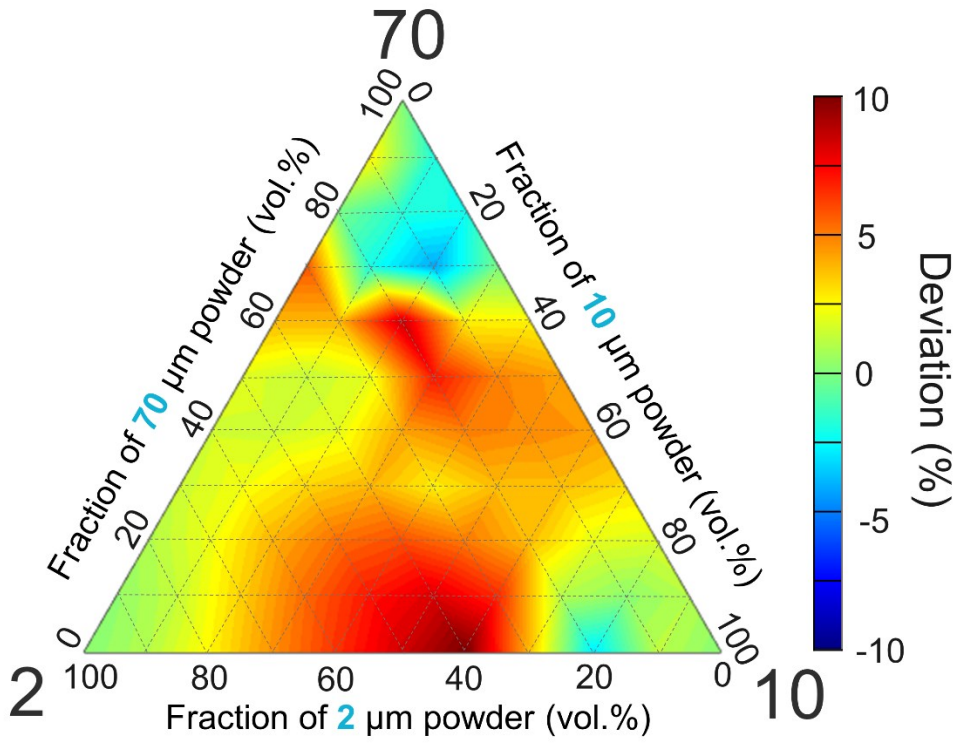

Figure 14. Deviation of trimodal mixture packing density predicted by the analytical model from measured tap density

5.3 Powder bed density and sintered density

Powder bed density and sintered density for different component powders and multimodal mixtures are shown in Table 4 and Figure 15. Standard deviation for the sintered density of 70-µm powder is not shown because the samples were very brittle after sintering and only one sample was available for the density measurement. The powder bed density achieved by multimodal mixtures is higher than that by their component powders in most cases. There are two exceptions: (1) the powder bed density of the 70/10 bimodal mixture is lower than that of 70-µm powder and (2) the powder bed density of the 10/2 bimodal mixture is lower than that of 10-µm powder. A possible reason is that the reduced flowability of the mixtures led to a nonuniform spreading of the powder bed and consequently a lower powder bed density. The trimodal mixture achieves the

largest powder bed density (60.1%) among all of the investigated powders and mixtures. However, the powder bed density was still lower than the tap density.

Sintered density achieved by multimodal mixtures is higher than that by their corresponding component powders in most cases. Although sintering improved the density, the finally achieved density was still significantly lower than the full density. A reason is that the powder bed density is far below the modeled packing density and the tap density. It indicates that the powder spreading process could be significantly improved to reach the ideal case. It also means that new models are needed to directly model the powder spreading process and predict the powder bed density, for example, with the discrete element method. Another reason could be that these powders have a low sinterability.

Table 4. Mixing fraction, powder bed density, and sintered density

Powder or mixture	Mixing fraction (vol.%)	Powder bed density (%)	Sintered density (%)
2	/	39.7 ± 0.9	46.8 ± 1.0
10	/	51.1 ± 0.7	57.5 ± 0.3
70	/	58.2 ± 0.7	60.5
10/2	66.3:33.7	45.2 ± 0.9	50.7 ± 0.9
70/10	67.7:32.3	53.6 ± 1.2	64.8 ± 0.8
70/2	70.0:30.0	59.5 ± 0.9	64.3 ± 3.7
70/10/2	61.3:21.1:17.6	60.1 ± 0.1	66.1 ± 0.8

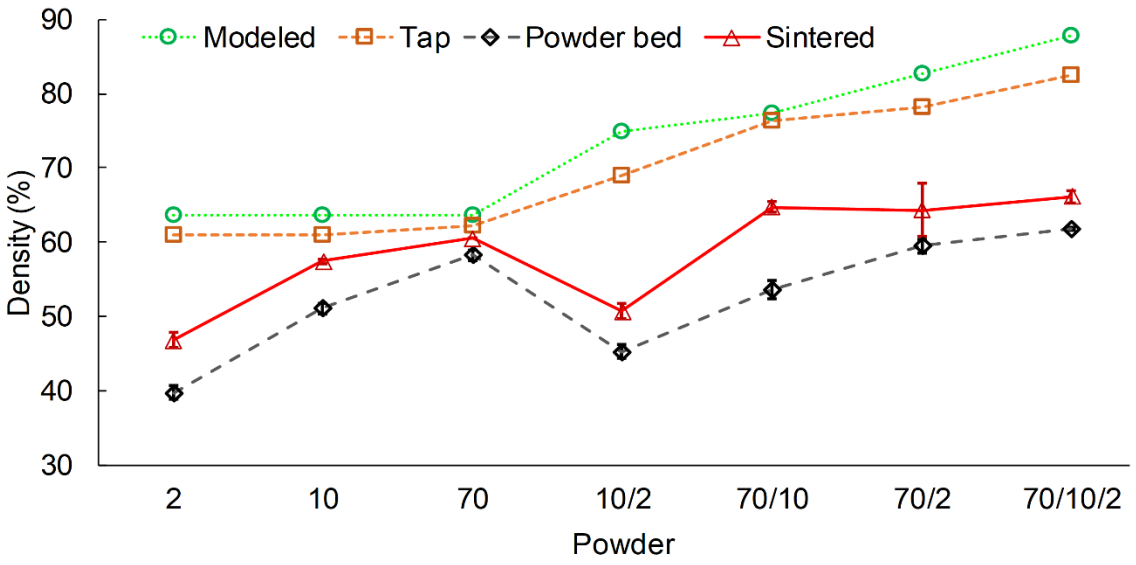

Figure 15. Various densities achieved by component powders and multimodal mixtures

5.4 Sintered microstructure

Figures 16 and 17 show the microstructure of sintered samples from component powders and multimodal mixtures, respectively. In a multimodal mixture, the voids among coarse particles are filled with fine particles, which has increased the powder bed density and the sintered density. For example, in the case of the 70/10/2 trimodal mixture, the 10-µm particles fill the voids among the 70-µm particles and 2-µm particles fill the remaining voids between 70-µm and 10-µm particles, which has led to the highest powder bed density and sintered density among all powders in this work.

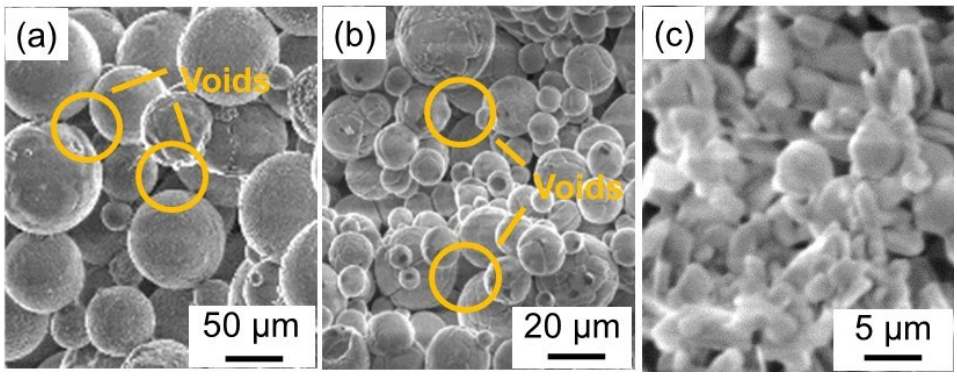

Figure 16. Microstructure of sintered samples from component powders: (a) 70 μm, (b) 10 μm, and (c) 2 μm.

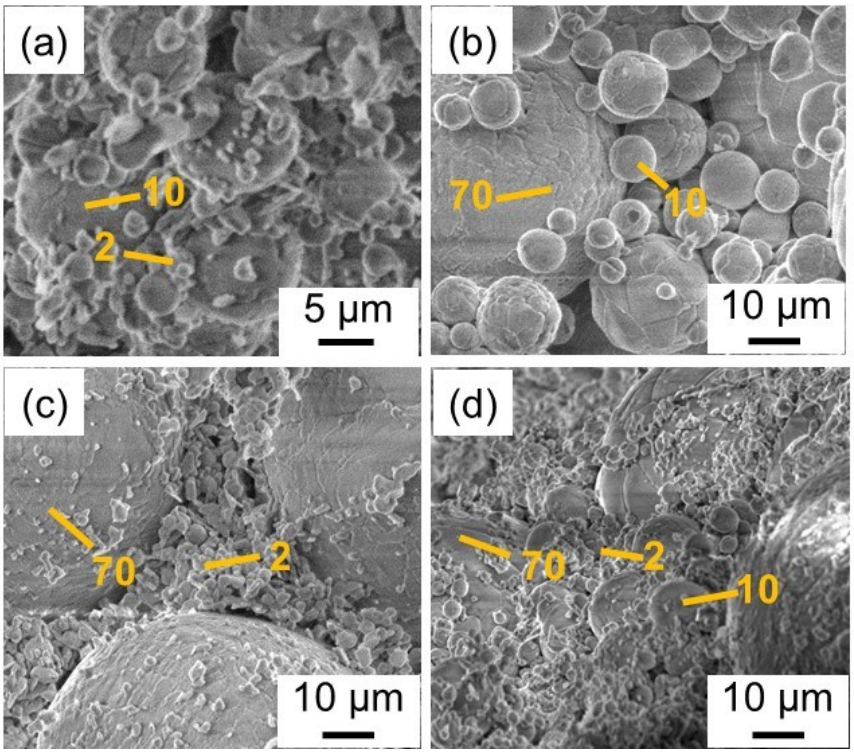

Figure 17. Microstructure of sintered samples from multimodal mixtures: (a) 10/2, (b) 70/10, (c) 70/2, and (d) 70/10/2.

6 Conclusions

This work investigated the effects of particle size distribution on density of a densely packed powder, powder bed density, and sintered density in binder jetting. Analytical results showed that there existed an optimal mixing fraction to achieve the maximum mixture packing density. Both a lower component particle size ratio (fine to coarse) and a larger component packing density ratio (fine to coarse) led to a larger maximum mixture packing density. Before mixing, the critical component packing density ratio can be used to decide whether the mixing method is effective. The dependence of the optimal mixing fraction and maximum mixture packing density on the

component particle size ratio and component packing density ratio was plotted and can be used as theoretical tools to select parameters for the mixing method. Experimental results of tap density were consistent with the aforementioned analytical predictions. In addition, experimental measurements showed that the powder bed density and thus the sintered density were improved by multimodal mixtures compared with component powders in most cases. However, there is still large room to improve the powder bed density and thus the sintered density.

Acknowledgements

This material is based upon work supported by the National Science Foundation under Grant No. 1762341.

References

[1] ASTM International, 2015, "ISO/ASTM 52900:2015 - Additive Manufacturing — General Principles — Terminology."

[2] Ziaee, M., and Crane, N. B., 2019, "Binder Jetting: A Review of Process, Materials, and Methods," Addit. Manuf., **28**, pp. 781–801.

[3] Du, W., Ren, X., Pei, Z., and Ma, C., 2020, "Ceramic Binder Jetting Additive Manufacturing: A Literature Review on Density," J. Manuf. Sci. Eng., **142**(4), pp. 1–66.

[4] Li, M., Du, W., Elwany, A., Pei, Z., and Ma, C., 2020, "Metal Binder Jetting Additive Manufacturing: A Literature Review," J. Manuf. Sci. Eng., **142**(9), pp. 1–45.

[5] Ma, C., Pei, Z., Ren, X., and Du, W., 2019, "Hierarchical Compositions for the Additive Manufacturing of Materials."

[6] Miao, G., Du, W., Moghadasi, M., Pei, Z., and Ma, C., 2020, "Ceramic Binder Jetting Additive Manufacturing: Effects of Granulation on Properties of Feedstock Powder and Printed and Sintered Parts," Addit. Manuf., **36**, p. 101542.

[7] Zocca, A., Colombo, P., Gomes, C. M., and Günster, J., 2015, "Additive Manufacturing of Ceramics: Issues, Potentialities, and Opportunities," J. Am. Ceram. Soc., **98**(7), pp. 1983–2001.

[8] "ExOne | Binder Jetting Technology" [Online]. Available: https://www.exone.com/en-US/case-studies/what-is-binder-jetting. [Accessed: 21-Sep-2019].

[9] Sachs, E., Cima, M., and Cornie, J., 1990, "Three-Dimensional Printing: Rapid Tooling and Prototypes Directly from a CAD Model," CIRP Ann. - Manuf. Technol., **39**(1), pp. 201–204.

[10] Sachs, E., Cima, M., Williams, P., Brancazio, D., and Cornie, J., 1992, "Three Dimensional Printing: Rapid Tooling and Prototypes Directly from a CAD Model," J. Eng. Ind., **114**(4), pp. 481–488.

[11] Díaz-Moreno, C. A., Lin, Y., Hurtado-Macías, A., Espalin, D., Terrazas, C. A., Murr, L. E., and Wicker, R. B., 2019, "Binder Jetting Additive Manufacturing of Aluminum Nitride Components," Ceram. Int., **45**(11), pp. 13620–13627.

[12] Maleksaeedi, S., Eng, H., Wiria, F. E., Ha, T. M. H., and He, Z., 2014, "Property Enhancement of 3D-Printed Alumina Ceramics Using Vacuum Infiltration," J. Mater. Process. Technol., **214**(7), pp. 1301–1306.

[13] Du, W., Ren, X., Ma, C., and Pei, Z., 2019, "Ceramic Binder Jetting Additive Manufacturing: Particle Coating for Increasing Powder Sinterability and Part Strength," Mater. Lett., **234**, pp. 327–330.

[14] Miyanaji, H., Zhang, S., Lassell, A., Zandinejad, A. A., and Yang, L., 2016, "Optimal Process Parameters for 3D Printing of Porcelain Structures," Procedia Manuf., **5**, pp. 870–887.

[15] Butscher, A., Bohner, M., Doebelin, N., Galea, L., Loeffel, O., and Müller, R., 2013, "Moisture Based Three-Dimensional Printing of Calcium Phosphate Structures for Scaffold Engineering," Acta Biomater., **9**(2), pp. 5369–5378.

[16] Vorndran, E., Moseke, C., and Gbureck, U., 2015, "3D Printing of Ceramic Implants," MRS Bull., **40**(2), pp. 127–136.

[17] Moghadasi, M., Du, W., Li, M., Pei, Z., and Ma, C., 2020, "Ceramic Binder Jetting Additive Manufacturing: Effects of Particle Size on Feedstock Powder and Final Part Properties," Ceram. Int., **46**(10), pp. 16966–16972.

[18] Sun, C., Tian, X., Wang, L., Liu, Y., Wirth, C. M., Günster, J., Li, D., and Jin, Z., 2017, "Effect of Particle Size Gradation on the Performance of Glass-Ceramic 3D Printing Process," Ceram. Int., **43**(1), pp. 578–584.

[19] Bai, Y., Wagner, G., and Williams, C. B., 2017, "Effect of Particle Size Distribution on Powder Packing and Sintering in Binder Jetting Additive Manufacturing of Metals," J. Mater. Sci. Eng., **139**, pp. 1–6.

[20] Kwan, A. K. H., Wong, V., and Fung, W. W. S., 2015, "A 3-Parameter Packing Density Model for Angular Rock Aggregate Particles," Powder Technol., **274**, pp. 154–162.

[21] Miao, G., Du, W., Pei, Z., and Ma, C., 2019, "Binder Jetting Additive Manufacturing of Ceramics: Analytical and Numerical Models for Powder Spreading Process," *ASME 2019 14th International Manufacturing Science and Engineering Conference, MSEC 2019*, American Society of Mechanical Engineers (ASME), Erie, PA.

[22] Stovall, T., de Larrard, F., and Buil, M., 1986, "Linear Packing Density Model of Grain

Mixtures," Powder Technol., **48**(1), pp. 1–12.

[23] Kwan, A. K. H., and Fung, W. W. S., 2009, "Packing Density Measurement and Modelling of Fine Aggregate and Mortar," Cem. Concr. Compos., **31**(6), pp. 349–357.

[24] de Larrard, F., 1999, *Concrete Mixture Proportioning: A Scientific Approach*, E & FN Spon, London.

[25] Scott, G. D., 1960, "Packing of Spheres: Packing of Equal Spheres," Nature, **188**(4754), pp. 908–909.

[26] German, R. M., 1989, *Particle Packing Characteristics*, Metal Powder Industries Federation, Princeton.

[27] Yu, A. B., Bridgwater, J., and Burbidge, A., 1997, "On the Modelling of the Packing of Fine Particles," Powder Technol., **92**(3), pp. 185–194.

[28] Abdullah, E. C., and Geldart, D., 1999, "The Use of Bulk Density Measurements as Flowability Indicators," Powder Technol., **102**(2), pp. 151–165.

[29] ASTM International, 2015, "B527-15: Standard Test Method for Tap Density of Metal Powders and Compounds."

[30] Rahaman, M. N., 2003, *Ceramic Processing and Sintering*, CRC Press, New York.

[31] Melcher, R., Travitzky, N., Zollfrank, C., and Greil, P., 2011, "3D Printing of Al2O3/Cu-O Interpenetrating Phase Composite," J. Mater. Sci., **46**(5), pp. 1203–1210.

[32] Gu, H., Gong, H., Dilip, J. J. S., Pal, D., Hicks, A., Doak, H., and Stucker, B., 2014, "Effects of Powder Variation on the Microstructure and Tensile Strength of Ti6Al4V Parts Fabricated by Selective Laser Melting," *Proceedings of the 25th Annual International Solid Freeform Fabrication Symposium*, Austin, TX, pp. 4–6.

[33] Kwan, A. K. H., Chan, K. W., and Wong, V., 2013, "A 3-Parameter Particle Packing Model Incorporating the Wedging Effect," Powder Technol., **237**, pp. 172–179.